



## Behavior of Copper Removal by CMP and Its Correlation to Deposit Structure and Impurity Content

Hsien-Ping Feng,<sup>a,\*</sup> Jeng-Yu Lin,<sup>a,\*\*</sup> Ming-Yung Cheng,<sup>b</sup> Yung-Yun Wang,<sup>a</sup> and Chi-Chao Wan<sup>a,\*\*</sup>

<sup>a</sup>Department of Chemical Engineering, National Tsing-Hua University, Hsinchu 300, Taiwan

<sup>b</sup>Department of Materials Science and Engineering, National Chiao Tung University, Hsinchu 300, Taiwan

Knowledge of the removal behaviors of various electroplated copper films during chemical mechanical polishing (CMP) is important for thickness control and defect generation. In this paper, we investigate the effect of current density and impurities incorporated in blanket and pattern wafer by potentiodynamic polarization method, X-ray diffraction, and secondary ion mass spectroscopy. Defect count was decided by the optical scan method and scanning electron microscopy reviewing. Removal rate and corroded pits were found to decrease with increasing (111)/(200) ratio because (111), the close-packed plane of the face-centered cubic structure, has strong chemical resistance during polishing. Furthermore, incorporated impure atoms, such as carbon, chloride, and sulfur, tend to weaken grain boundaries to generate more corroded pits but do not affect removal rate. Besides, geometric constraint induces concentrated impurities to restrict copper grain growth and induce fast oxide growth rate, resulting in high dishing performance.

© 2007 The Electrochemical Society. [DOI: 10.1149/1.2801394] All rights reserved.

Manuscript submitted April 21, 2007; revised manuscript received September 24, 2007.  
Available electronically November 6, 2007.

Copper has replaced aluminum as the interconnect metal of integrated circuits due to its higher electrical conductivity and superior electromigration resistance. Electroplating was adopted as the primary method for Cu deposition. Microstructure control of electroplated Cu became a focus of interest during chemical mechanical polishing (CMP). Polishing performance, including defect generation and removal rate, has a high correlation to copper microstructure and slurry characteristics. Lee and Wong<sup>1</sup> reported that a strong correlation between stress change and texture development was found for Cu deposit during self-annealing and post-thermal annealing. For face-centered cubic (fcc) metal films, orientation of the lowest surface energy is (111) and that of the lowest elastic strain energy is (100).<sup>2,3</sup> As the film stress exceeds a critical value, the (111) texture diminishes and the (200) texture enhances to minimize the total energy.<sup>4,5</sup> Film stress is also affected by the bond strength of the Cu/TaN barrier interface.<sup>6</sup> Strong interface bonding leads to large stress and thus degrades (111) texture.<sup>7,8</sup> Moreover, Zhang reported that impurities originated from plating additives and its intermediate cathodic products, such as bis(3-sulfopropyl)disulfide or 3-mercapto-1-propanesulfonate, are trapped into the deposit to retard grain growth in narrow lines.<sup>9</sup> Suppressor complex derives more impurities to incorporate in deposit and impurities increase with reducing line width. According to the model of curvature-enhanced accelerator coverage (CEAC) that was recently developed by West et al. and Moffat et al., Cl-suppressor complexes are distributed on the copper seed surface by nonpreferential adsorption at an early stage of plating. Copper superfilling is dominated by the surface adsorption of additives and the surface-to-volume ratio inside the narrower trenches is higher than that in the wider trenches.<sup>10,11</sup>

Furthermore, copper-surface chemistry plays an important role in the CMP process. Jindal and Babu<sup>12</sup> reported that the mechanism of copper removal in slurries is through the formation of a porous oxide layer, leading to a higher removal rate and reduced friction from a softened surface layer. In general, oxide or metal removal of CMP can usually be simulated by the Preston equation ( $RR = kPV + RR_0$ ), where  $RR$  is the material removal rate,  $k$  is the Preston constant,  $P$  is the applied wafer pressure,  $V$  is the average linear pad-wafer velocity, and  $RR_0$  represents the dynamic etch rate of the material in the absence of pressure and velocity.<sup>13,14</sup> CMP involves complex interactions between the polishing substrate, polishing pad,

chemical slurry, and abrasive agents. Ye et al.<sup>15</sup> proposed that CMP of copper has two components: (i) the mechanical abrasion by the abrasive and (ii) the dissolution of the abraded material from the copper surface by chemical action of the slurry. Many reports were related to the chemical effect or the mechanical parameters, and empirical equations were established to describe the polishing behavior.<sup>15-17</sup>

However, the performance of various copper films during CMP are not yet well understood, involving film texture and impurity effect. The purpose of this article is to study the characteristics of various copper films during CMP. A removal mechanism and defect performance, based on electrochemical measurement and surface analytic technology, are proposed. Increased knowledge regarding the interaction between plated film properties and polishing behaviors can improve the stability of CMP thickness control and reduce defect generation.

### Experimental

**Wafer preparation.**— Blanket wafers used in this study were 8 in. Si(100) wafers with 100 nm thermal oxide/30 nm TaN/150 nm Cu seed layer/1000 nm copper deposit, where the TaN and Cu seed layers were deposited by physical vapor deposition (PVD) without vacuum breaking. Patterned wafers with different line widths were generated by optical lithography and etch processes.

**Plating and polishing.**— Electrodeposition was carried out on Novellus Sabre hardware using 15°C bath control and 180°C anneal condition (60 s). Electroplating studies were performed in an acid copper sulfate electrolyte containing 50 g/L copper metal, 200 g/L sulfuric acid, and 100 mg/L chloride ion. Two additives, 1 mL/L of a proprietary organic accelerator additive of the sulfide type [Shipley Company, similar to bis(sodium-sulfopropyl)disulfide (SPS)] and 10 mL/L of a proprietary organic additive suppressor of the polyglycol type [Shipley Company, similar to poly(ethylene glycol)], were added to electrolyte. An Applied-Material Mirra polisher was used to polish these wafers. Polishing conditions are at head of 70 rpm, platen of 70 rpm, and down force of 2 psi. Two-step polishing processes were carried out, including the first stage with copper polishing and then Ta and oxide polishing. The copper polishing slurry was prepared with 3.1 wt % fumed aluminum particle and an acid solution with pH 3–5, which contained ingredients, including 0.2 wt % hydrogen peroxide, 1 wt % passivation agent [benzotriazole (BTA)], and a phthalic acid salt which is commonly used in

\* Electrochemical Society Student Member.

\*\* Electrochemical Society Active Member.

<sup>z</sup> E-mail: nt-fong@hotmail.com

**Table I.** List of film properties for deposits with different current conditions.

Current density (mA/cm <sup>2</sup> )	$\rho$ Variation <sup>a</sup> (%)	Thickness shrinkage (Å)	(111)/(200)	FWHM <sup>b</sup>
5	21.1	1.87	8.3	0.579
20	22.4	2.52	5.8	0.577
33	23.7	3.08	4.5	0.578

<sup>a</sup>  $\rho$  variation:  $(\rho_{\text{before anneal}} - \rho_{\text{after anneal}}) / \rho_{\text{after anneal}}$

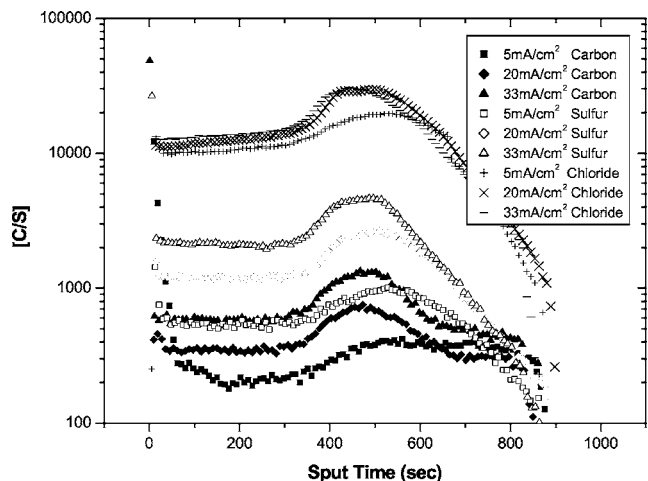
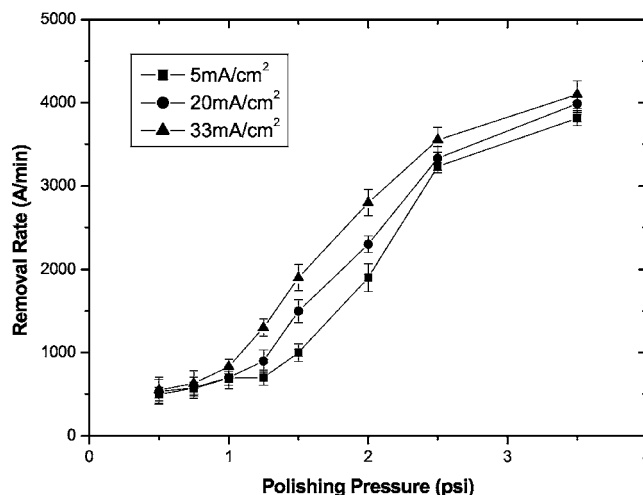
<sup>b</sup> The value of fwhm is inversely proportional to the grain size and was held at the same level with the increase of current density.

metal CMP slurries as a buffering and chelating agent. The peroxide and passivation agents were used as oxidizer and inhibitor for this study, respectively.

**Measurement.**—Static potentiodynamic polarization was performed using an EG&G Princeton Applied Research model 273 potentiostat/galvanostat system. A platinum foil was used as the counter electrode and a saturated calomel electrode (SCE) was used as the reference electrode in a standard three-electrode system. The removal rate of Cu film was measured by the four-point probe method using a 49 point line scan on a Prometrix resistance measurement tool. Dishing/erosion performance was monitored by Tenor Alpha-step 500 Surface Profiler. X-ray diffraction (XRD) was applied to determine the Cu orientation. Impurities of Cu deposit, including carbon and sulfur atoms, were detected by secondary ion mass spectrometer (SIMS) analysis. The optical scan method (KLA) was used to detect surface defect of Cu film after CMP. The defect types were classified and determined with an AMAT SEMVision reviewing tool.

### Results and Discussion

We focus on understanding the substrate effect of different copper surfaces for removal rate (global behavior) and corroded pits (local behavior). First, we use current density as the controlled parameter to produce copper films of different microstructures based on previous studies.<sup>18,19</sup> Resistivity variation, thickness shrinkage value, and orientation ratio for three deposits with different current conditions are summarized in Table I. Figure 1 also shows SIMS results of carbon, sulfur, and chloride content, which are originated from plating additives and intermediate cathodic products. Raising the current density obviously induces more vacancies/dislocations and impurities, resulting in more tensile stress.<sup>1</sup> Grain growth for

**Figure 1.** SIMS analysis (carbon/sulfur/chloride) for deposits from different current densities.**Figure 2.** Relationship between removal rate of copper and polishing pressure.

grain boundaries elimination and orientation evolution for film-stress release are common approaches to reach low surface energy via anneal treatment.<sup>1,20-22</sup> Table I shows that deposit of high current density causes a large thickness shrinkage but the same final grain size [the same value of full width at half-maximum (fwhm) means similar grain boundaries elimination]. It implies that increasing current density induces more texture evolution. High plating current density produces copper deposit with a low (111)/(200) ratio and high impurity content.

The relation between removal rate and polishing pressure is shown in Fig. 2, which is divided into two regions for non-Preston and Preston behavior.<sup>23</sup> Three-type deposits produced from different current densities are tested. In Fig. 2, a deposit of low current density (5 mA/cm<sup>2</sup>) has a large threshold pressure at about 1.2 psi, resulting in a lower polishing rate than in the cases of high current density. Below threshold pressure, removal rate is close to a constant, which is the etch rate of the material without pressure and velocity  $RR_0$ . Above threshold pressure, removal rate increases with increasing mechanical force. Hence, it can be simulated by the Preston equation ( $RR = kPV + RR_0$ ). Initially, removal rate slowly increases as pressure rises because low pressure is insufficient to abrade the inhibitor layer. Further increase of pressure raises temperature between slurry and copper surface to naturally speed up etching and  $\text{CuO}_x$  formation. Until exceeding threshold pressure, the high etching rate and porous  $\text{CuO}_x$  interface, which can reduce frictional force among the pad, slurry, and wafer surface, cause a linear relationship between removal rate and applied pressure. Chen and Wang<sup>23</sup> proposed a schematic plot of the layer structure to illustrate this phenomenon. As described above, the increase of removal rate results from the continuous copper dissolution, the formation of a  $\text{Cu}_2\text{O}$  passive layer promoted by the hydroxyl radical, and the consequent mechanical abrasion. Based on Cu 2p X-ray photoelectron spectroscopy (XPS) spectra, the metal copper (0)/cuprous (+1) oxide signal of high current density (33 mA/cm<sup>2</sup>) is weaker than that of low current density (5 mA/cm<sup>2</sup>) after polishing, as shown in Fig. 3. The peak of Cu/Cu<sub>2</sub>O is relatively strong for deposits without polishing. It indicates that the signal of cupric (+2) oxide (hydroxide) of deposit plated from high current density is relatively intense after polishing. It also means that deposits obtained from different plating current conditions have different surface chemical reactions even though under the same polishing condition. Figure 4 displays the static potentiodynamic polarization curves for deposits from three plating current densities. Among these curves, it is found that the higher the plating current density, the higher the corrosion po-

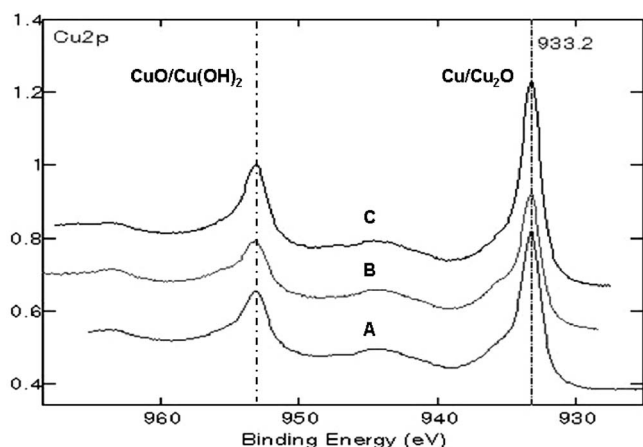


**Figure 3.** XPS Cu 2p spectra of copper samples for (A) 1000 nm deposit plated at 5 mA/cm<sup>2</sup> after 2 psi polishing for 60 min, (B) 1000 nm deposit plated at 33 mA/cm<sup>2</sup> after 2 psi polishing for 60 min, and (C) 1000 nm deposit without polishing.

tential and corrosion current. This implies that deposit plated from high current density has relatively low chemical resistance against surface reaction with slurry.

*Effect of crystal orientation.*—The wide variation of polishing behavior of deposits plated from different current densities implies that plating conditions can significantly affect the crystal orientation and impurity content in the deposit. Based on Fig. 2, we can most effectively differentiate the removal rate of these three cases at 2 psi polishing pressure. Hence, the following experiments were done under 2 psi. In general, grain boundaries are easily corroded to generate pits, which is also true in our case, as shown in Fig. 5, because copper atoms are more loosely packed along the grain boundaries than in the crystal lattices. Therefore, corroded pits are an important index for localized corrosion phenomenon. So we studied the effect of (111)/(200) ratio in copper deposit on the global removal rate and local corroded pits. The results shown in Fig. 6 illustrate that both removal rate and pit count significantly decreased with increasing (111)/(200) ratio, which means that the copper polished surface with high (111)/(200) ratio has strong chemical resistance.<sup>24,25</sup> For fcc thin films, (111) texture favors surface and interfacial energy minimization, whereas (200) texture favors strain energy minimi-

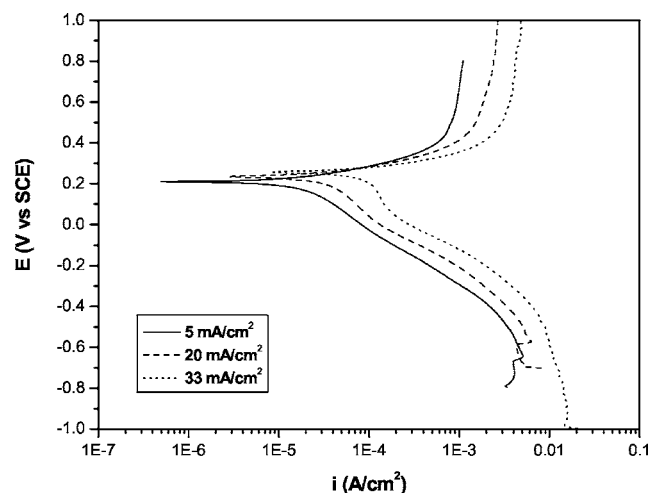


**Figure 4.** Potentiodynamic polarization curves for copper films with various plating current densities in slurry.

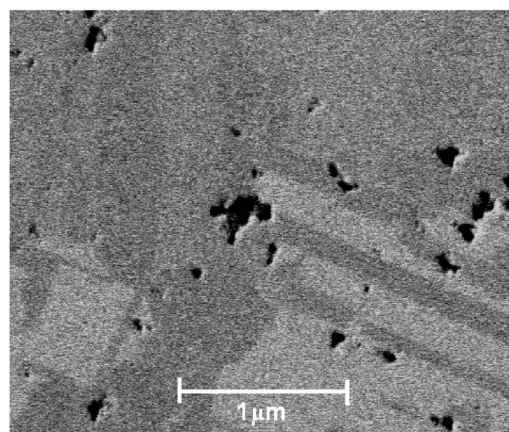


**Figure 5.** FIB images for pits on copper surface after polishing.

zation.<sup>2,3</sup> So (111) texture should exhibit stronger chemical resistance than other planes because (111) is the closest packed plane in the fcc structure.

*Effect of impurity.*—Plating baths with four different additive concentrations were chosen to deposit Cu films with different impurities but with the same texture because the current density was kept constant at 20 mA/cm<sup>2</sup>. As listed in Table II, data from SIMS analysis and XRD measurement show a wide variation of carbon/sulfur content and almost the same (111)/(200) ratio, which implies that the amount of additive can affect the impurity content in the deposit but is insufficient to change copper orientation for blanket thin film. Results shown in Fig. 7 reveal that the removal rate is not influenced

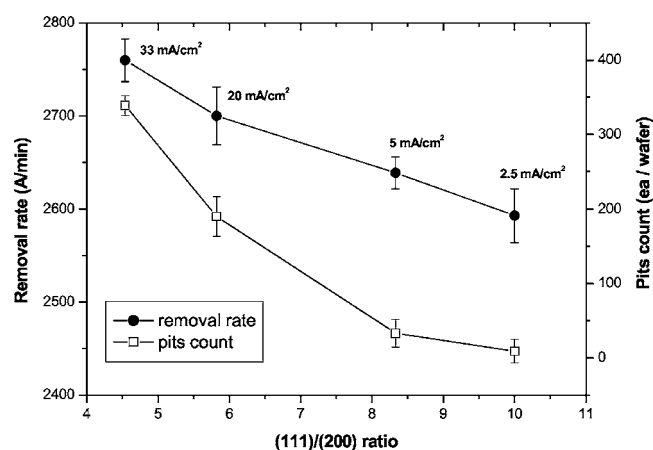


**Figure 6.** Removal rate and pit defect vs copper deposits with different (111)/(200) ratios which were obtained from different current densities.

**Table II.** List of film properties for 20 mA/cm<sup>2</sup> 1000 nm with four additive concentrations.

Film	XRD analysis		SIMS analysis <sup>a</sup>		
	(111)/(200)	FWHM	Carbon	Sulfur	Chloride
A <sup>b</sup>	5.83	0.577	1.0	1.0	1.0
B	5.85	0.576	1.3	1.7	1.5
C	5.85	0.577	1.9	2.7	2.3
D	5.82	0.577	2.5	3.5	2.9

<sup>a</sup> SIMS analysis results compared with film A as standard "1".

<sup>b</sup> A: 1 mL/L accelerator, B: 3 mL/L, C: 5 mL/L, and D: 7 mL/L accelerator.



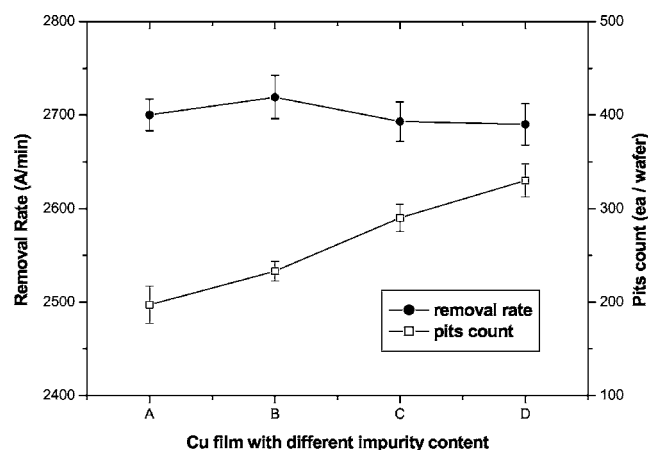


**Figure 7.** Removal rate and void defect vs copper deposits with different impurities (A < B < C < D).

by carbon/sulfur impurity to any appreciable extent, but the pit count increases steadily with increasing impurity content. One reason could be that removal rate reflects the performance of the whole copper surface, including grains and grain boundaries, but the pit defect is mainly related to the condition of grain boundaries where impurities are favorably aggregated. So, impurities are insufficient to influence the removal rate because grain boundaries constitute a relatively small area where only local pitting shows its significance. Hence, copper film with high impurity could generate more defects during polishing because impurities can weaken Cu grain boundaries.

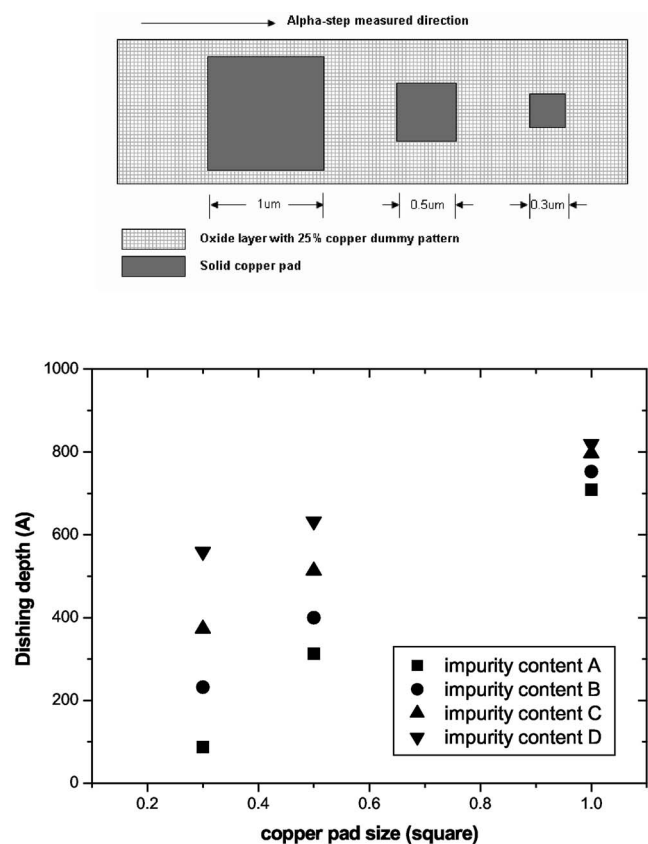


**Figure 8.** Dishing depth vs impurity content for different solid pad structures (A < B < C < D).

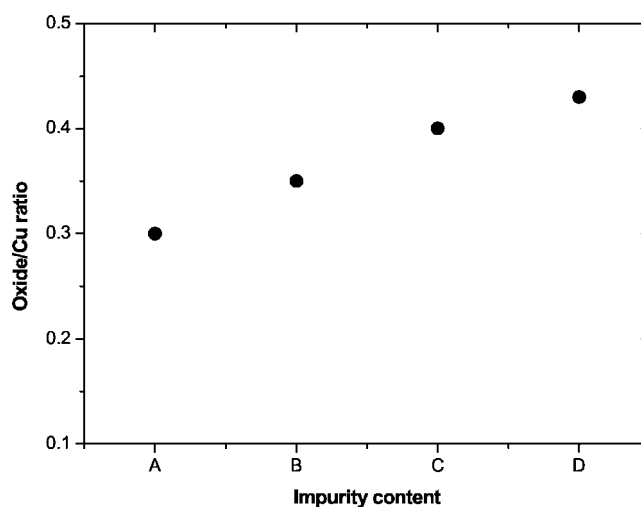


**Figure 9.** Oxide/Cu ratio vs copper deposits with different impurities at 60 s polishing (A < B < C < D).

*Effect of geometry.*— We needed to further consider the geometry effect on microstructural evolution for pattern wafer. The most important index is dishing/erosion, which is directly related to sheet resistance of interconnect metal. Previous studies reported that plating electric field causes impure atoms to concentrate at the trench corner, which in turn alters grain growth and orientation after annealing.<sup>9</sup> As described above, chemical resistance is associated with film orientation. Alpha-step was used to measure dishing depth on three copper pad sizes ( $1 \times 1$ ,  $0.5 \times 0.5$ , and  $0.3 \times 0.3$   $\mu\text{m}$ ) of pattern wafer. Figure 8 reveals that dishing depth increases with increasing impurity and the increase becomes more significant as the copper-pad dimension diminishes. Dishing depth decreases with reducing additives to prove that sufficient impure atoms can change surface chemical resistance. In brief, pads of smaller dimension tend to be more sensitive to impurities. These results could be explained by assuming that a small dimension has a high concentration of impure atoms because of geometric constraint.<sup>9</sup> Cu et al. reported that oxide growth occur slowly on the S-free Cu surface as compared with the S-modified copper surface.<sup>26</sup> Thereby, we use Cu  $2p_{3/2}$  and O 1s XPS intensities to derive the oxide/Cu ratio vs impurities, as shown in Fig. 9. These data indicate that Cu surfaces with more impurities induce fast oxide growth rate. In summary, geometric constraints lead concentrated impurities in a narrow line to induce fast oxide growth rate, resulting in large dishing depth.

### Conclusion

Electroplating under different current densities generated copper films with different textures and impurity content, which in turn had different removal rates and pitting behaviors after CMP. Potentiodynamic polarization method study proves that corrosion current value increases with decreasing (111)/(200) ratio. The characteristics of various copper films from our studies are summarized below.

1. Removal rate and pit defects decrease with increasing (111)/(200) ratio. High (111)/(200) ratio has strong chemical resistance during polishing. XPS analysis shows that a deposit of high current density has strong  $\text{Cu}_2\text{O}$  intensity as compared with that of low current density. It represents that deposits obtained from different plating current conditions have different responses to surface chemical reaction by the same polishing process.

2. Although impurities are not able to influence the removal rate, they are an important factor for pitting generation because the impure atoms can weaken Cu grain boundaries.

3. Geometric constraint causes uneven impurity distribution, which influences oxide growth rate to change the chemical resistance of copper surface.

National Tsing Hua University assisted in meeting the publication costs of this article.

### References

1. H. Lee, S. S. Wong, and S. D. Loptain, *J. Appl. Phys.*, **93**, 3796 (2003).
2. H. L. Wei, R. K. Zheng, G. H. Wen, and X. X. Zhang, *Appl. Phys. Lett.*, **80**, 2290 (2002).
3. T. Hara, H. Toida, and Y. Shimura, *Electrochem. Solid-State Lett.*, **6**, G98 (2003).
4. Q. T. Jiang and M. E. Thomas, *J. Vac. Sci. Technol. B*, **19**, 762 (2001).
5. S. M. Rossnagel and T. S. Kuan, *J. Vac. Sci. Technol. A*, **20**, 1911 (2002).
6. C. Detavernier, D. Deduytsche, R. L. Van Meirhaeghe, J. De Baerdemaeker, and C. Dauwe, *Appl. Phys. Lett.*, **82**, 1863 (2003).
7. K. R. Hebert, *J. Electrochem. Soc.*, **148**, C726 (2001).
8. S. Nakayama, A. Kimura, M. Shibata, S. Kuwabata, and T. Oskai, *J. Electrochem. Soc.*, **148**, B467 (2001).
9. W. Zang, *J. Electrochem. Soc.*, **152**, C832 (2005).
10. C. West, S. Mayer, and J. Reid, *Electrochem. Solid-State Lett.*, **4**, C50 (2001).
11. T. P. Moffat, D. Wheeler, W. H. Huber, and D. Josell, *Electrochem. Solid-State Lett.*, **4**, C26 (2001).
12. A. Jindal and S. V. Babu, *J. Electrochem. Soc.*, **151**, G709 (2004).
13. Y. Homma, *J. Electrochem. Soc.*, **153**, G587 (2006).
14. J. Hernandez, P. Wrschka, and G. S. Oehrlein, *J. Electrochem. Soc.*, **148**, G389 (2001).
15. Y. Ye, R. Biswas, A. Bastawros, and A. Chandra, *Appl. Phys. Lett.*, **81**, 1875 (2002).
16. Z. Li, K. Ina, P. Lefevre, I. Koshiyama, and A. Philipossian, *J. Electrochem. Soc.*, **152**, G299 (2005).
17. T. Du, D. Tamboli, V. Desai, and S. Seal, *J. Electrochem. Soc.*, **151**, G230 (2004).
18. T. Hara, K. Sakata, and Y. Yoshida, *Electrochem. Solid-State Lett.*, **5**, C41 (2002).
19. M. W. Lane, C. E. Murray, F. R. McFeely, P. M. Vereecken, and R. Rosenberg, *Appl. Phys. Lett.*, **83**, 2330 (2003).
20. C. Detavernier, S. Rossnagei, C. Noyan, S. Guha, C. Cabral, Jr., and C. Lavoie, *J. Appl. Phys.*, **94**, 2874 (2003).
21. Q.-T. Jiang and M. E. Thomas, *J. Vac. Sci. Technol. B*, **19**, 762 (2001).
22. J. M. E. Harper, C. Cabral, Jr., P. C. Andricacos, L. Gignac, I. C. Noyan, K. P. Rodbell, and C. K. Hu, *J. Appl. Phys.*, **86**, 2516 (1999).
23. K.-W. Chen and Y. L. Wang, *J. Electrochem. Soc.*, **154**, H41 (2007).
24. J. Y. Lin, C. C. Wan, Y. Y. Wang, and H. P. Feng, *J. Electrochem. Soc.*, **154**, D139 (2007).
25. J. Y. Lin, Y. Y. Wang, C. C. Wan, H. P. Feng, and M. Y. Cheng, *Electrochem. Solid-State Lett.*, **10**, H23 (2007).
26. H.-C. Cu, G. Seshadri, and J. A. Kelber, *J. Electrochem. Soc.*, **147**, 558 (2008).